Signaling Delays Preclude Defects in Lateral Inhibition Patterning

David S. Glass, Xiaofan Jin, and Ingmar H. Riedel-Kruse*
Department of Bioengineering, Stanford University, Stanford, California 94305, USA
(Received 17 April 2015; revised manuscript received 25 November 2015; published 22 March 2016)

Lateral inhibition represents a well-studied example of biology's ability to self-organize multicellular spatial patterns with single-cell precision. Despite established biochemical mechanisms for lateral inhibition (e.g., Delta-Notch), it remains unclear how cell-cell signaling delays inherent to these mechanisms affect patterning outcomes. We investigate a compact model of lateral inhibition highlighting these delays and find, remarkably, that long delays can ensure defect-free patterning. This effect is underscored by an interplay with synchronous oscillations, *cis* interactions, and signaling strength. Our results suggest that signaling delays, though previously posited as a source of developmental defects, may in fact be a general regulatory knob for tuning developmental robustness.

DOI: 10.1103/PhysRevLett.116.128102

Many multicellular organisms produce spatially differentiated tissues with single-cell precision [1–3]. Several mechanisms may explain such precision, including morphogen gradients [4], Turing patterning [5], and lateral inhibition [6,7]. However, patterning fidelity—the scarcity of observed defects relative to an ideal pattern—remains challenging to explain given gene expression noise [2], varying environments [8] and signal transduction delays [9]. Here we specifically examine the role of intercellular signaling delays in lateral inhibition and show that, in fact, delays can guarantee high fidelity despite opposing conclusions in closely related contexts [9].

Lateral inhibition signaling is responsible for checkered patterns in a diverse set of processes such as vertebrate neurogenesis [10–14], plant hair distribution [15], and insect bristle formation [16–18] [Fig. 1(a)]. In the classic metazoan Delta-Notch system [Fig. 1(b)], Notch receptor is cleaved upon binding to membrane-displayed Delta ligand on a neighboring ("*trans*") cell. Notch's remaining intracellular fragment, a transcription factor, then downregulates Delta [19] and controls cell fate. Moreover, recent work [20–23] shows that Notch and Delta mutually inactivate on the same ("*cis*") cell surface. These interactions putatively speed patterning [9,24], but no definitive role has been established [9,20,22,24–27].

Signaling pathways such as Delta-Notch accumulate delays [28] through protein production, trafficking, and other processes. Despite known roles in other patterning mechanisms [29–31], delays remain largely ignored in lateral inhibition models [7,12,26]. As exceptions, Veflingstad, *et al.* [32] and Momiji & Monk [33] did include explicit delays, noting their contribution to oscillatory behavior, but did not examine their effects on spatial defects. Barad, *et al.* studied the related problem of differentiating a single cell from a two-cell cluster, and noted that long delays impede differentiation assuming either hysteresis or a differentiation time cutoff [9]. Meanwhile, we examine spatial patterning in many-celled tissues without these conditions and find that long delays then in fact minimize spatial defects.

Mathematical model.—To simplify our analysis of lateral inhibition, we abstract *trans* regulation into a motif [Fig. 1(c)] in which a single protein species x downregulates like proteins in neighboring cells. While consistent with mechanistic models (Sec. S1–2 [34]), this motif bundles biochemical details such as mRNA transcription and protein binding, and their associated time scales, into a

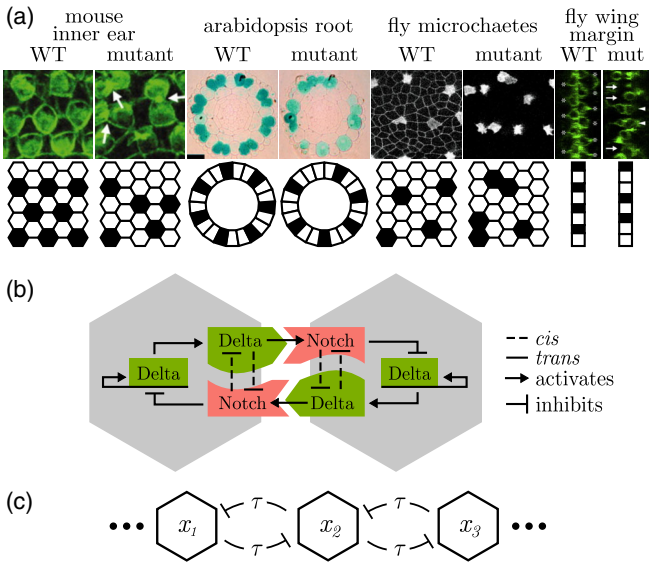

FIG. 1. Lateral inhibition demonstrates high fidelity and single-cell precision using delayed signaling pathways. (a) Biological examples (from left: Refs. [13,15,17,18]) and our corresponding models with and without defects. Longer-range models (root and microchaetes) require next-nearest neighbor interactions. (b) Notch-Delta signaling pathway, where Delta effectively downregulates neighboring Delta. (c) Simplified *trans*-only delay model of (b), equivalent to Eq. (1). Black cells in (a) correspond to high x_i.

single repression term with effective delay τ. This motif translates directly into our governing equation:

$$\dot{x}_i(t) = p_0 + \frac{\alpha k^n}{k^n + (\sum_j^N x_j(t-\tau))^n} - \beta x_i(t) + \sigma\zeta(t), \quad (1)$$

where x_i is the ith cell's protein level, p_0 its basal production rate, α its maximum production rate, k the regulatory half-maximal input, n the cooperativity, $1/\beta$ the characteristic protein decay time, N the number of nearest neighbors, and $\sigma\zeta = \mathcal{N}(0,\sigma)$ a white noise function simulating noisy gene expression. The sum over j represents accumulated repression from N neighboring cells. Equation (1) and some initial analysis parallels work from Veflingstad, *et al.* [32] and Momiji & Monk [33], who explored dynamics primarily in the two-cell model.

Normalizing concentration $X = x/k$ and time $T = t/(1/\beta)$ leaves the nondimensional form

$$\dot{X}_i(T) = \epsilon + \frac{\eta}{1 + (\sum_j^N X_j(T-\gamma))^n} - X_i(T) + \rho\zeta(T). \quad (2)$$

Signaling strength $\eta = \alpha/k\beta$, leakage $\epsilon = p_0/k\beta$, and noise $\rho = \sigma/k\beta$ all denote production per decay time. Normalized delay $\gamma = \tau\beta$ denotes the ratio of delay to decay times. We disregard ϵ, as leaky gene expression is tightly regulated in the Delta-Notch pathway [47], and is overwhelmed by noise ($\epsilon \ll \rho$). Outcomes are largely unaffected by cooperativity n (Sec. S3 [34]), except that $n < 2$ (1D) and $n < 3$ (2D hexagonal lattice) fail to pattern; biological n typically ranges from 1–4 [48]. Thus just two parameters, γ and η, dictate the patterning dynamics. Biologically relevant protein levels x lie within the repressive dynamic range near k, so X and hence $\eta = \max(X)$ are $\sim O(1)$, with $\rho \lesssim O(1)$. Literature values also support biological $\gamma \sim O(1)$ (Sec. S4 [34]).

Parameter exploration.—Delay differential equations such as Eq. (2) are challenging to study analytically due to complex dynamics [49–53] and infinite-dimensional initial condition spaces [54]. Instead, we numerically integrated Eq. (2) to steady state from low, mostly homogeneous X as biologically relevant initial conditions (Sec. S5 [34]), for simplicity in a 1D tissue of M cells with circular boundary conditions. For each (γ, η), we recorded the error rate, defined as the percentage of simulations that yielded defects, defined in turn as interruptions to the regular alternating pattern [Fig. 2(c)]. We also recorded differentiation time T_{steady}, defined as the time until the system reaches steady state. Three regions emerge [Fig. 2(a)]: (1) high error rates for low γ, (2) transient oscillations leading to defect-free patterning for high γ, and (3) unpatterned tissues for low η. This suggests that large delays provide robust patterning, albeit with reduced speed [Fig. 2(b)], consistent with observations that delay-induced oscillations slow differentiation [32] and qualitatively similar to the idea of error-free iterative selection [9].

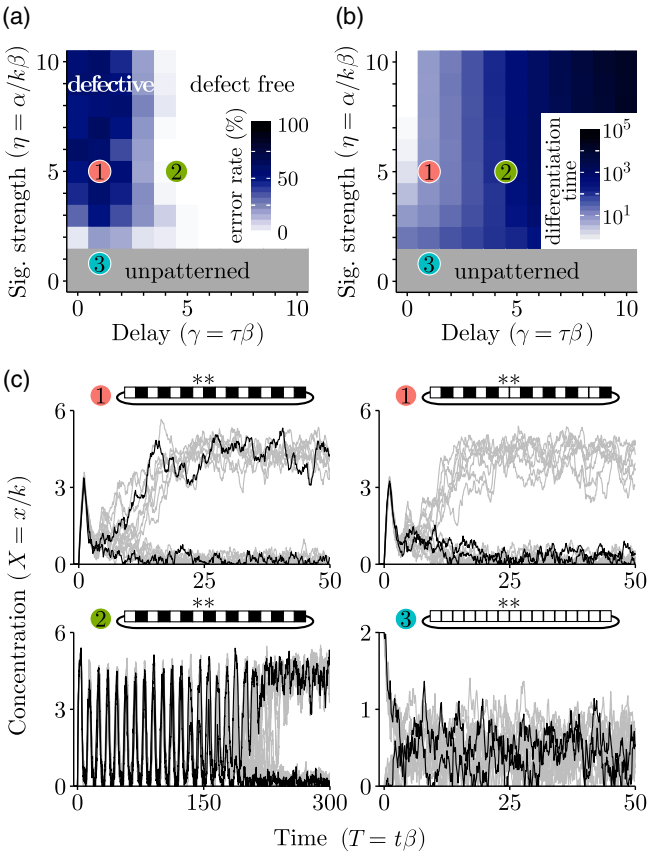

FIG. 2. Increased signaling delay leads to vanishing error rate. (a) Error rates and (b) differentiation times showing regions where tissues are (1) often defective and lack oscillations, (2) always perfect following oscillations, and (3) unpatterned even with initial patterning. (c) Example time traces from these regions with their steady state patterns. Starred cells have traces highlighted in black. See Sec. S6 [34] for kymographs. $\rho^2 = 0.1$, $M = 16$, $n = 2$.

Cell-local analysis.—We examined local interactions to explain the vanishing error rate for high γ. In this regime, whole-tissue, synchronous oscillations persist for many cycles, with slight cell-to-cell differences superimposed. To highlight these differences, we define the normalized relative concentration $r = \delta^2[\mathbf{X}]/\sigma_{\delta^2[\mathbf{X}]}$, with $\delta^2[\mathbf{X}] = 2X_i - X_{i+1} - X_{i-1}$ (Sec. S7 [34]), and find that cells organize into domains [Fig. 3(a), pink rectangles] wherein cells with high and low r alternate. Mismatched domains meet at a boundary cell (pink arrows) with $r \sim 0$. Larger domains contain cells with larger $|r|$, their stronger regulation causing boundary cells to align polarity with the larger of their adjacent domains. The corresponding contraction of smaller domains leads to defect annihilation (green arrows). Fitting time to annihilation vs initial defect spacing d yields $T_{\text{annihilate}} \sim d^2$ (Sec. S8 [34]), comparable to defect diffusion within Ising models [55] despite different underlying mechanisms.

Perfect patterning occurs if correction time, defined as the time needed for all defects to annihilate, is shorter

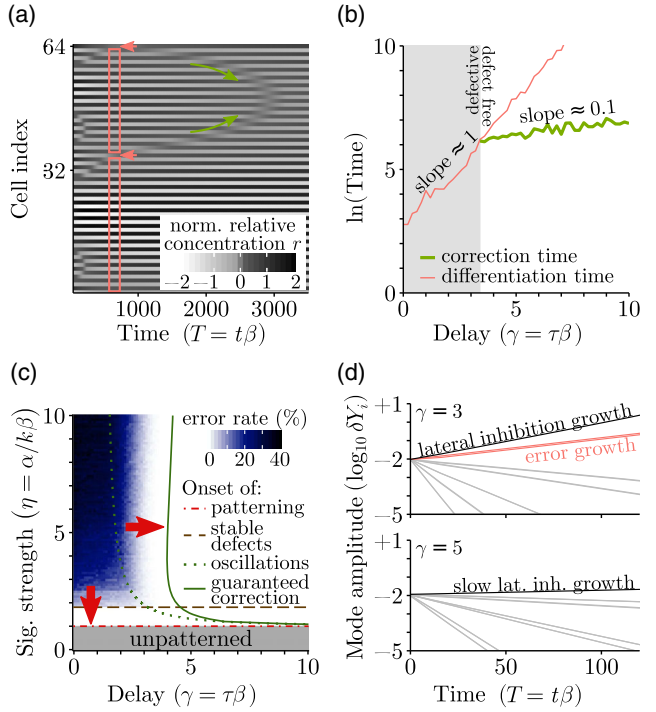

FIG. 3. Defect resolution is guaranteed past a critical γ, with global stability changes driving local defect annihilation. (a) Patterned domains (pink rectangles) have larger normalized relative concentrations r (note contrast differences) and push domain boundaries (pink arrows) together (green arrows). See Sec. S7 for absolute concentrations [34]. (b) Pattern correction time grows much slower with γ than differentiation time, allowing time for defect resolution at high γ. $\eta = 5$. (c) Theoretical boundary curves match simulations. Arrows point towards decreasing error rate, driven by large delays or weak signaling. (d) All modes around limit cycle $\hat{X}(T)$ become stable for high γ except the lateral inhibition mode, which grows slowly (oscillations filtered out for clarity). $\rho = 0$ for $T > 0$, $n = 2$. $M = 16$ (b), (c), (d), and $M = 64$ (a).

than differentiation time. Differentiation time grows faster in γ than correction time. These two times meet near the point where the observed error rate vanishes (Fig. 3(b), Sec. S9 [34]), suggesting that large delays slow differentiation so defects have sufficient time to be resolved.

Global mode analysis.—Beyond this qualitative, cell-local picture of delay-driven defect resolution, we next examined quantitative, whole-tissue transitions across the (γ, η) parameter space [Fig. 3(c)]. We sampled at high resolution with 1000 noise-free ($\rho = 0$) replicates for easy comparison to analytics. In particular, we explain four observations: (i) patterning requires a minimum signaling strength, (ii) error rates are low just beyond this minimum, and (iii) increasing delay past critical boundaries causes oscillations while (iv) reducing error rates.

We start by linearizing about the unpatterned steady state $X_i = X^*$, yielding

$$\delta\dot{\mathbf{X}}(T) + \eta m B \delta\mathbf{X}(T-\gamma) + \delta\mathbf{X}(T) = 0, \tag{3}$$

where the constant $m(X^*) = n(NX^*)^{n-1}/[1+(NX^*)^n]^2$, and matrix elements $B_{ij} = 1$ if cells i and j are neighbors and 0 otherwise. Diagonalizing $B = SDS^{-1}$ leads to M equations for the components of $\delta\mathbf{Y} = S^{-1}\delta\mathbf{X}$:

$$\delta\dot{Y}_i(T) + \eta m D_i \delta Y_i(T-\gamma) + \delta Y_i(T) = 0, \tag{4}$$

where D_i is B's ith eigenvalue. Eigenvectors of B denote modes of concentration deviation from X^*, and δY_i is the amplitude of the ith mode. Of particular note are the lateral inhibition $(1,-1,1,-1,\ldots)^\top$ and uniform $(1,1,1,\ldots)^\top$ modes, corresponding to $D_i = -2$ and $D_i = +2$, respectively. Applying the ansatz $\delta Y_i(T) = Ae^{\lambda T}$ yields a transcendental characteristic equation

$$\lambda + \eta m D_i e^{-\gamma\lambda} + 1 = 0. \tag{5}$$

The system $\delta\mathbf{Y}$ becomes unstable when any δY_i becomes unstable, either at $\lambda = 0$ (a saddle-node bifurcation) or $\lambda = i\omega$ (a Hopf bifurcation). The former simplifies Eq. (5) to $\eta m D_i = -1$, which given $\dot{X}_i = 0$, yields $\eta = X^*[1 + (NX^*)^n]$ and the condition

$$\eta = -\frac{nD_i}{N^2}\left(-\frac{nD_i}{N} - 1\right)^{-(n+1)/n}. \tag{6}$$

The lowest η with unstable X^* occurs at $D_i = -2$, where unpatterned tissue shifts towards lateral inhibition, every cell growing away from its neighbors [red dot-dashed line in Fig. 3(c)]. This explains observation (i), that a homogeneous steady state is stable only below a threshold.

Numerically testing stability around nonhomogeneous spatial patterns reveals similar bifurcations, purely dependent on signaling strength η. The boundary for lateral inhibition stability coincides with the red Eq. (6) patterning threshold, while no defective patterns (Sec. S12 [34]) become stable until higher η [dashed brown line in Fig. 3(c)]. For η between the brown and red lines, only lateral inhibition steady states are stable regardless of delay. In agreement with observation (ii), low and in fact zero error rates are found just beyond the minimum signaling strength required for patterning.

Analyzing the Hopf bifurcation $\lambda = i\omega$, and separating the real and imaginary parts of Eq. (5), leads to

$$\eta = -\frac{nD_i}{N^2}\cos\Omega\left(-\frac{nD_i}{N}\cos\Omega - 1\right)^{-(n+1)/n},$$
$$\gamma = -\Omega\cot\Omega, \tag{7}$$

with $\Omega = \gamma\omega$ used to parameterize the curve. In the direction of increasing (γ, η), the first δY_i to become unstable corresponds to $D_i = +2$, shown as the dotted green curve in Fig. 3(c). Consistent with simulation, to the right of this Hopf bifurcation a nearly uniform tissue

oscillates synchronously near a limit cycle $\hat{X}(T)$, explaining observation (iii) that increasing delay causes oscillations.

To understand how these oscillations are driven towards differentiation, we linearized around the cycle $\hat{X}(T)$, yielding exactly Eq. (4) but with time-varying $m(T)$, obtained numerically using Eq. (2). Subsequent numerical integration of Eq. (4) reveals that solutions $\delta Y_i(T)$ grow or decay exponentially with superimposed oscillations.

Increasing γ causes amplitudes δY_i to decay for all modes around $\hat{X}$ except lateral inhibition [Fig. 3(d)], which grows more slowly but remains unstable. The γ where lateral inhibition becomes the only growing mode [solid green curve in Fig. 3(c)] coincides with sharply decreased error rate, and explains (iv) that increasing delay reduces error rates. This essentially *guarantees* perfect patterning for initially low, near-homogeneous tissues, which are drawn into $\hat{X}$ oscillations and escape only via the lateral inhibition mode. The dynamics then converge to just one pair of stable fixed points (i.e., perfect patterning) out of very many (defective) alternatives ($\gg 10^3$ for $M = 64$).

Slow growth of the lateral inhibition mode at high γ also explains the tradeoff between error rate and speed. In fact, the tradeoff is so extreme that patterning using high γ to preclude defects is too slow ($T_{\text{steady}} \gtrsim 500$) to be biologically relevant. In contrast, a *Drosophila* tissue patterns within ~14 hrs [3,17,56,57] with signaling protein decay time ~10 min [58–62], a normalized patterning time of $T_{\text{steady}} \approx 84$. Alongside similar estimates in other organisms (Sec. S4 [34]), this suggests that a secondary mechanism exists to accelerate defect resolution.

cis interactions.— Previous work suggests that *cis* interactions [Fig. 1(b)] may speed patterning [26], increase signaling cooperativity [24–26], and expand the patterned parameter space [26]. To see if *cis* interactions could solve the tradeoff, we added a variable decay rate f to Eq. (2):

$$\dot{X}_i(T) = \epsilon + \frac{\eta}{1 + (\sum_j^N X_j(T-\gamma))^n} - X_i(T) - f(X_i, X_j(T-\gamma))X_i(T) + \rho\zeta(T), \quad (8)$$

$$f = \frac{k_1}{k_2 + X_i(T)} \frac{(\sum_j^N X_j(T-\gamma))^n}{1 + (\sum_j^N X_j(T-\gamma))^n}, \quad (9)$$

where k_1 and k_2 determine the strength and sensitivity of *cis* effects, respectively. Intuitively, f describes accelerated degradation in cells with lower concentration and whose neighbors had higher concentrations in the past. This effectively modulates delay dynamically [$\gamma' = \gamma(1+f)$], and is consistent with the mechanistic model of Sprinzak, *et al.* [26] (Sec. S13 [34]).

Simulations of Eq. (9) (Fig. 4, Sec. S14 [34]) show the same regimes as Fig. 2, but with lower η patterning threshold and smaller γ sufficient for proper patterning.

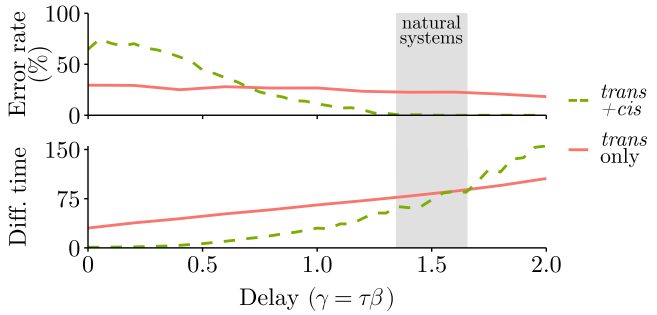

FIG. 4. *cis* interactions combined with delays enable fast yet robust patterning. Error rate and differentiation time for patterning with and without *cis* interactions. Grayed region shows biologically relevant ($T_{\text{steady}} \lesssim 85$ [34], error rate $\lesssim 1\%$ [9]) parameters with *cis* interactions; no such parameters exist for *trans*-only regulation. $\eta = 5$, $k_1 = 10$, $k_2 = 1$, $\rho^2 = 0.1$, $M = 16$, $n = 2$.

Minimal robust differentiation time reduces to $T_{\text{steady}} \approx 80$, within our earlier estimate for real biological systems; other k_1, k_2, or M may decrease T_{steady} further. Thus we corroborate increased parameter robustness [26] and show that *cis* interactions allow robust, yet fast, patterning.

Tissue geometries.—Finally, we extended our model to more general tissue sizes and geometries. We found that larger tissue size M requires longer delay or lower signaling strength to guarantee defect-free patterning. Accordingly, the high-γ and low-η defect-free phase boundaries for M cells in Fig. 3(c) have analogous curves in larger tissues corresponding to fewer defects spaced M cells apart (Sec. S15 [34]). We also tested a 2D hexagonal lattice, and included next-nearest neighbors in both 1D and 2D to model filopodia [27]. The latter yields longer spatial patterns with neighboring "high" cells in 2D [Fig. 1(a) microchaetes]. In every scenario, large delays preclude defects, and *cis* interactions increase the optimal robust speed. Parameter spaces for 2D and filopodia are squeezed, however, with "large delays" ~3× smaller than before. Additionally, these tissues exhibit stable limit cycles of $\hat{X}(T)$ for $\gamma \gtrsim 2$, suggesting further mechanisms for 2D and filopodia to enforce differentiation if large delays are used.

Discussion.—Based on our theoretical results, we propose several mechanisms for how real biological systems can avoid defects. Tissues can use delay-driven oscillations to ensure patterning fidelity, but incur longer differentiation time ($T_{\text{steady}} \sim M^{2.03\pm0.12}$ with *cis* interactions, Sec. S15 [34]). Indeed, oscillations have been observed in Delta-Notch systems [12,63], although such oscillations have not been shown to be synchronous or tied to defect resolution. Alternatively, tissues can use weak signaling to ensure fidelity, but become susceptible to molecular noise as differences diminish between "high" and "low" cells. They also lose robustness to parameter variation, which easily abolishes patterning or increases error rates. These tradeoffs become biologically infeasible in very large

tissues, where ensuring fidelity requires either exceedingly long delays or impeccably tuned signaling strength. Natural systems in this regime such as sensory organs [1,3] seem to first differentiate quickly (low γ, high η), and then remove resulting defects by cellular motion, division, or apoptosis [64].

On a practical note, the predicted tradeoffs among delays, signaling strengths, and patterning fidelity can be measured phenotypically using modified Delta-Notch systems [13,65] in, e.g., *Drosophila* microchaete patterning [9,16]). Varying intron lengths [28] to adjust mRNA processing time (τ) and protein degradation tags [66] to tune the decay time ($1/\beta$) both affect normalized delay $\gamma = \tau/(1/\beta)$. Modulated promoter strength (α) and operator sensitivity (k) [67] similarly tune signaling strength $\eta = \alpha/k\beta$. Such experiments would solidify signaling delays as an overlooked developmental control knob, and we hope our work encourages such further exploration into the role of delays in controlling patterning fidelity.

We would like to thank D. Sprinzak, L. Morelli, J. Axelrod, A. Choksi, J. Glass, and J. Reinhardt for their feedback and discussions. This work was supported in part by Stanford Bio-X Bowes and NSERC PGS fellowships.

D. S. G. and X. J. contributed equally to this work.

*To whom correspondence should be addressed.
ingmar@stanford.edu

[1] C. B. Brachmann and R. L. Cagan, Patterning the fly eye: The role of apoptosis, Trends Genet. **19**, 91 (2003).

[2] T. Gregor, D. Tank, E. Wieschaus, and W. Bialek, Probing the limits to positional information, Cell **130**, 153 (2007).

[3] A. Koto, E. Kuranaga, and M. Miura, Apoptosis ensures spacing pattern formation of Drosophila sensory organs, Curr. Biol. **21**, 278 (2011).

[4] C. Nusslein-Volhard and E. Wieschaus, Mutations affecting segment number and polarity in Drosophila, Nature (London) **287**, 795 (1980).

[5] H. Meinhardt, Turing's theory of morphogenesis of 1952 and the subsequent discovery of the crucial role of local self-enhancement and long-range inhibition, Interface Focus **2**, 407 (2012).

[6] P. Sternberg, Lateral inhibition during vulval induction in Caenorhabditis elegans, Nature (London) **335**, 551 (1988).

[7] J. Collier, N. Monk, P. Maini, and J. Lewis, Pattern formation by lateral inhibition with feedback: A mathematical model of delta-notch intercellular signalling, J. Theor. Biol. **183**, 429 (1996).

[8] Y.-J. Jiang, B. L. Aerne, L. Smithers, C. Haddon, D. Ish-Horowicz, and J. Lewis, Notch signalling and the synchronization of the somite segmentation clock, Nature (London) **408**, 475 (2000).

[9] O. Barad, D. Rosin, E. Hornstein, and N. Barkai, Error minimization in lateral inhibition circuits, Sci. Signal. (Online) **3**, ra51 (2010).

[10] C. Haddon *et al.*, Multiple delta genes and lateral inhibition in zebrafish primary neurogenesis, Development (Cambridge, England) **125**, 359 (1998).

[11] Y. Wakamatsu, T. Maynard, and J. Weston, Fate determination of neural crest cells by NOTCH-mediated lateral inhibition and asymmetrical cell division during gangliogenesis, Development (Cambridge, England) **127**, 2811 (2000).

[12] R. Kageyama, T. Ohtsuka, H. Shimojo, and I. Imayoshi, Dynamic Notch signaling in neural progenitor cells and a revised view of lateral inhibition, Nat. Neurosci. **11**, 1247 (2008).

[13] H. Togashi, K. Kominami, M. Waseda, H. Komura, J. Miyoshi, M. Takeichi, and Y. Takai, Nectins establish a checkerboard-like cellular pattern in the auditory epithelium, Science **333**, 1144 (2011). Figure reprinted with permission from AAAS.

[14] P. Formosa-Jordan, M. Ibaes, S. Ares, and J. M. Frade, Regulation of neuronal differentiation at the neurogenic wavefront, Development (Cambridge, U.K.) **139**, 2321 (2012).

[15] M. M. Lee and J. Schiefelbein, Cell pattern in the Arabidopsis root epidermis determined by lateral inhibition with feedback, Plant Cell **14**, 611 (2002). Figure reprinted with permission from ASPB.

[16] P. Simpson, Lateral inhibition and the development of the sensory bristles of the adult peripheral nervous system of Drosophila, Development (Cambridge, England) **109**, 509 (1990).

[17] M. Cohen, M. Georgiou, N. L. Stevenson, M. Miodownik, and B. Baum, Dynamic filopodia transmit intermittent Delta-Notch signaling to drive pattern refinement during lateral inhibition, Dev. Cell **19**, 78 (2010). Figure reprinted with permission from Elsevier.

[18] M. Takemura and T. Adachi-Yamada, Cell death and selective adhesion reorganize the dorsoventral boundary for zigzag patterning of Drosophila wing margin hairs, Dev. Biol. **357**, 336 (2011). Figure reprinted with permission from Elsevier.

[19] K. G. Guruharsha, M. W. Kankel, and S. Artavanis-Tsakonas, The Notch signalling system: recent insights into the complexity of a conserved pathway, Nat. Rev. Genet. **13**, 654 (2012).

[20] A. Yaron and D. Sprinzak, The cis side of juxtacrine signaling: a new role in the development of the nervous system, Trends Neurosci. **35**, 230 (2012).

[21] A. Miller, E. Lyons, and T. Herman, cis-Inhibition of Notch by endogenous Delta biases the outcome of lateral inhibition, Curr. Biol. **19**, 1378 (2009).

[22] G. Falivelli, E. Mathes Lisabeth, E. R. de la Torre, G. Perez-Tenorio, G. Tosato, O. Salvucci, E. B. Pasquale, and R. Zhou, Attenuation of eph receptor kinase activation in cancer cells by coexpressed ephrin ligands, PLoS One **8**, e81445 (2013).

[23] M. Fortini, Notch signaling: the core pathway and its posttranslational regulation, Dev. Cell **16**, 633 (2009).

[24] D. Sprinzak, A. Lakhanpal, L. LeBon, L. A. Santat, M. E. Fontes, G. A. Anderson, J. Garcia-Ojalvo, and M. B. Elowitz, Cis-interactions between Notch and Delta generate

mutually exclusive signalling states, Nature (London) **465** (2010).
[25] I. Becam, U. Fiuza, A. Arias, and M. Milán, A role of receptor Notch in ligand cis-inhibition in Drosophila, Curr. Biol. **20**, 554 (2010).
[26] D. Sprinzak, A. Lakhanpal, L. LeBon, J. Garcia-Ojalvo, M. B. Elowitz, and D. Thieffry, Mutual inactivation of Notch receptors and ligands facilitates developmental patterning, PLoS Comput. Biol. **7** (2011).
[27] J. Axelrod, Delivering the lateral inhibition punchline: It's all about the timing, Sci. Signal. (Online) **3**, pe38 (2010).
[28] I. A. Swinburne, D. G. Miguez, D. Landgraf, and P. A. Silver, Intron length increases oscillatory periods of gene expression in animal cells, Genes Dev. **22**, 2342 (2008).
[29] J. Hsia, W. J. Holtz, D. C. Huang, M. Arcak, M. M. Maharbiz, and M. S. Alber, A feedback quenched oscillator produces turing patterning with one diffuser, PLoS Comput. Biol. **8**, e1002331 (2012).
[30] L. G. Morelli, S. Ares, L. Herrgen, C. Schröter, F. Jülicher, and A. C. Oates, Delayed coupling theory of vertebrate segmentation, HFSP J. **3**, 55 (2009).
[31] J. Lewis, Autoinhibition with transcriptional delay: A simple mechanism for the zebrafish somitogenesis oscillator, Curr. Biol. **13**, 1398 (2003).
[32] S. R. Veflingstad, E. Plahte, and N. A. Monk, Effect of time delay on pattern formation: Competition between homogenisation and patterning, Physica (Amsterdam) **207D**, 254 (2005).
[33] H. Momiji and N. A. M. Monk, Oscillatory Notch-pathway activity in a delay model of neuronal differentiation, Phys. Rev. E **80**, 021930 (2009).
[34] See Supplemental Material at http://link.aps.org/supplemental/10.1103/PhysRevLett.116.128102 for detailed methods and derivations, parameter and time scale estimates, further model parameter exploration, and a comparison to a mechanistic model. Supplements include Refs. [35–46]
[35] D. Sprinzak and M. B. Elowitz, Reconstruction of genetic circuits, Nature (London) **438**, 443 (2005).
[36] M. H. Glickman and A. Ciechanover, The ubiquitin-proteasome proteolytic pathway: Destruction for the sake of construction, Physiol. Rev. **82**, 373 (2002).
[37] M. Boareto, M. Kumar Jolly, M. Lu, J. N. Onuchic, C. Clementi, and E. Ben-Jacob, Jagged-Delta asymmetry in Notch signaling can give rise to a Sender/Receiver hybrid phenotype, Proc. Natl. Acad. Sci. U.S.A. **112**, E402 (2015).
[38] J. A. Drocco, O. Grimm, D. W. Tank, and E. Wieschaus, Measurement and perturbation of morphogen lifetime: Effects on gradient shape, Biophys. J. **101**, 1807 (2011).
[39] A. Ay *et al.*, Short-lived Her proteins drive robust synchronized oscillations in the zebrafish segmentation clock, Development (Cambridge, England) **140**, 3244 (2013).
[40] P. Maini and H. Othmer, *Mathematical Models for Biological Pattern Formation, The IMA Volumes in Mathematics and its Applications* (Springer, New York, NY, 2012).
[41] L. Couturier, M. Trylinski, K. Mazouni, L. Darnet, and F. Schweisguth, A fluorescent tagging approach in Drosophila reveals late endosomal trafficking of Notch and Sanpodo, J. Cell Biol. **207**, 351 (2014).
[42] L. I. Held Jr, *Imaginal Discs: The Genetic and Cellular Logic of Pattern Formation*, Developmental and Cell Biology Series (Cambridge University Press, Cambridge, England, 2005).
[43] F. Coumailleau, M. Fürthauer, J. A. Knoblich, and M. González-Gaitán, Directional Delta and Notch trafficking in Sara endosomes during asymmetric cell division, Nature (London) **458**, 1051 (2009).
[44] O. Cinquin, Is the somitogenesis clock really cell-autonomous? A coupled-oscillator model of segmentation, J. Theor. Biol. **224**, 459 (2003).
[45] P. J. Lanford, Y. Lan, R. Jiang, C. Lindsell, G. Weinmaster, and T. Gridley, M. W. Kelley, Notch signalling pathway mediates hair cell development in mammalian cochlea, Nat. Genet. **21**, 289 (1999).
[46] V. Munnamalai, T. Hayashi, and O. Bermingham-McDonogh, Notch prosensory effects in the Mammalian cochlea are partially mediated by Fgf20, J. Neurosci. **32**, 12876 (2012).
[47] S. D. Hooper, S. Boué, R. Krause, L. J. Jensen, C. E. Mason, M. Ghanim, K. P. White, E. EM. Furlong, and P. Bork, Identification of tightly regulated groups of genes during Drosophila melanogaster embryogenesis, Mol. Syst. Biol. **3**, 72 (2007).
[48] J. N. Weiss, The Hill equation revisited: Uses and misuses, FASEB J. **11**, 835 (1997).
[49] K. L. Cooke and Z. Grossman, Discrete delay, distributed delay and stability switches, J. Math. Anal. Appl. **86**, 592 (1982).
[50] J. M. Mahaffy, K. M. Joiner, and P. J. Zak, A geometric analysis of stability regions for a linear differential equation with two delays, Int. J. Bifurcation Chaos Appl. Sci. Eng. **05**, 779 (1995).
[51] U. Heiden *et al.*, Oscillatory modes in a nonlinear second-order differential equation with delay, J. Dyn. Differ. Equ. **2** (1990).
[52] J. Bélair and S. A. Campbell, Stability and bifurcations of equilibria in a multiple-delayed differential equation, SIAM J. Appl. Math. **54**, 1402 (1994).
[53] C. Gupta *et al.*, Transcriptional Delay Stabilizes Bistable Gene Networks, Phys. Rev. Lett. **111**, 058104 (2013).
[54] R. Bellman and K. L. Cooke, *Differential-Difference Equations, Mathematics in Science and Engineering* (Elsevier Science, New York, 1963).
[55] R. Bellman and K. L. Cooke, Diffusion annihilation in one dimension and kinetics of the Ising model at zero temperature, Phys. Rev. A **41**, 3258 (1990).
[56] M. Cohen, B. Baum, and M. Miodownik, The importance of structured noise in the generation of self-organizing tissue patterns through contact-mediated cell-cell signalling, J. R. Soc. Interface **8**, 787 (2011).
[57] V. Hartenstein and J. W. Posakony, A dual function of the Notch gene in Drosophila sensillum development, Dev. Biol. **142**, 13 (1990).
[58] A. Kicheva, P. Pantazis, T. Bollenbach, Y. Kalaidzidis, T. Bittig, F. Julicher, and M. Gonzalez-Gaitan, Kinetics of morphogen gradient formation, Science **315**, 521 (2007).
[59] R. Sancho, S. M. Blake, C. Tendeng, B. E. Clurman, J. Lewis, A. Behrens, and R. Kopan, Fbw7 repression by hes5 creates a feedback loop that modulates Notch-mediated

intestinal and neural stem cell fate decisions, PLoS Biol. **11**, e1001586 (2013).

[60] S. Das, *Handbook of Research on Computational Methodologies in Gene Regulatory Networks* (Medical Information Science Reference, Hershey, PA, 2009).

[61] A. Leier, K. Burrage, and P. Burrage, Stochastic Modelling and Simulation of Coupled Autoregulated Oscillators in a Multicellular Environment: The her1/her7 Genes, in *Computational Science—ICCS 2007*, edited by Y. Shi, G. van Albada, J. Dongarra, and P. Sloot, Lecture Notes in Computer Science Vol. 4487 (Springer, Berlin, Heidelberg, New York, 2007), pp. 778–785.

[62] E. C. Lai, G. A. Deblandre, C. Kintner, and G. M. Rubin, Drosophila neuralized is a ubiquitin ligase that promotes the internalization and degradation of delta, Dev. Cell **1**, 783 (2001).

[63] H. Shimojo, T. Ohtsuka, and R. Kageyama, Oscillations in notch signaling regulate maintenance of neural progenitors, Neuron **58**, 52 (2008).

[64] G. J. Podgorski, M. Bansal, and N. S. Flann, Regular mosaic pattern development: A study of the interplay between lateral inhibition, apoptosis and differential adhesion, Theor. Biol. Med. Model. **4**, 43 (2007).

[65] M. Matsuda, M. Koga, K. Woltjen, E. Nishida, and M. Ebisuya, Synthetic lateral inhibition governs cell-type bifurcation with robust ratios, Nat. Commun. **6**, 6195 (2015).

[66] A. Bachmair, D. Finley, and A. Varshavsky, In vivo half-life of a protein is a function of its amino-terminal residue, Science **234**, 179 (1986).

[67] M. R. Schlabach, J. K. Hu, M. Li, and S. J. Elledge, Synthetic design of strong promoters, Proc. Natl. Acad. Sci. U.S.A. **107**, 2538 (2010).